Influence of Co incorporation on morphological, structural, and optical properties of ZnO nanorods synthesized by chemical bath deposition

Iwan Sugihartono*[1], Novan Purwanto[1], Desy Mekarsari[1], Isnaeni[2], Markus Diantoro[3], Riser Fahdiran[1], Yoga Divayana[4] and Anggara Budi Susila[1]

*[1]Program Studi Fisika, FMIPA Universitas Negeri Jakarta,
Jl. Rawamangun Muka, Jakarta Timur 13220, Indonesia*
[2]National Research and Innovation Agency, KST BJ Habibie, South Tangerang, 15314 Indonesia
[3]Department of Physics, State University of Malang, Jl. Semarang No 5, Malang 65145, Indonesia
[4]Department of Electrical Engineering, Udayana University, Kampus Bukit Jimbaran, Bali 80361, Indonesia

Abstract. We have studied the structural and optical properties of the non-doped and Co 0.08 at.%, Co 0.02 at.%, and Co 0.11 at.% doped ZnO nanorods (NRs) synthesized using the simple low-temperature chemical bath deposition (CBD) method at 95°C for 2 hours. The scanning electron microscope (SEM) images confirmed the morphology of the ZnO NRs are affected by Co incorporation. As observed, the Co 0.08 at.% doped ZnO NRs have a larger dimension with an average diameter of 153.4 nm. According to the International Centre for Diffraction Data (ICDD) number #00-036-1451, the x-ray diffraction (XRD) pattern of non-doped and Co-doped ZnO NRs with the preferred orientation of ZnO NRs in the (002) plane possess polycrystalline hexagonal wurtzite structure with the space group P6$_3$mc. Optical absorbance indicates the Co 0.08 at.% doped ZnO NRs have stronger and blueshift bandgap energy (3.104 ev). The room temperature photoluminescence (PL) spectra of ZnO NRs exhibited excitonic-relates ultraviolet (UV) and defect-related green band (GB) emissions. By calculating the UV/GB intensity, the Co 0.08 at.% is the proper atomic percentage to have fewer intrinsic defects. We predict that Co-doped ZnO NRs induce a blueshift of near band edge (NBE) emission due to the Burstein-Moss effect. Meanwhile, the redshift of NBE emission is attributed to the modification of the lattice dimensions and exchange energy.

Keywords: bandgap energy; Co-doped ZnO NRs; morphology; NBE emission; polycrystalline hexagonal wurtzite

1. Introduction

ZnO is an II-VI semiconductor also common as piezoelectric material that extensively studied for the last two decades (Allahverdinejad Sarab *et al.* 2022). ZnO is a low-cost, non-toxic, earth-abundant, high chemical and thermal stability, high mechanical strength, and wide direct bandgap energy of 3.34eV, hence ZnO is promising material for broad optoelectronic applications

*Corresponding author, Ph.D., E-mail: isugihar@hotmail.com, iwan-sugihartono@unj.ac.id

(Demircan *et al.* 2023, Lehru *et al.* 2021, Movlarooy *et al.* 2018, Sugihartono *et al.* 2012). Moreover, ZnO has a strong exciton binding energy of 60 meV larger than thermal energy at room temperature (26meV) (Sugihartono *et al.* 2016, Tan *et al.* 2005).

ZnO nanorods (ZnO NRs) as one-dimensional (1D) nanostructures have great potential applications for low-dimension optoelectronic devices (Yang *et al.* 2007). As reported, ZnO NRs can be synthesized by some methods i.e., metal-organic chemical vapor deposition (MOCVD) (Sugihartono *et al.* 2018), chemical bath deposition (CBD) (Sugihartono *et al.* 2019), hydrothermal process (Roza *et al.* 2020), a facile low-temperature solution method (Ta *et al.* 2018), etc.

As a 1D nanostructure, ZnO NRs should have a smaller size than the exciton Bohr radius. Hence, most researchers believed the quantum confinement in ZnO nanorods is responsible for the shifting of luminescence. It is called blue shift (Yang *et al.* 2007, Sugihartono *et al.* 2018, Sugihartono *et al.* 2019, Roza *et al.* 2020, Ta *et al.* 2018, Yu *et al.* 2003). However, in diameter, the ZnO nanorods mostly are much larger than the Bohr radius (Sugihartono *et al.* 2018, Jin *et al.* 2003, Song and Lim 2006). Moreover, the anomalous of blue-shift in ZnO nanorods with a diameter larger than exciton the Bohr radius is related to the Burstein-Moss band filling effect under the excitation of the high-energy electron beam (Yang *et al.* 2007). On the other hand, the luminescence properties of ZnO can be used to study the evolution of electronic defects (Lima *et al.* 2001). To the best of our knowledge, zinc interstitial (Zni) and oxygen vacancy (Vo) are dominant nature defects that attribute to the n-type behavior. Others reported the nature of the defects to depend on morphology, structure, particle size, composition, and crystallinity which play an important role in the optical properties of ZnO (Sugihartono *et al.* 2019, Lima *et al.* 2001, Tan *et al.* 2005).

Our previous results stated that doping is one of the important parameters to modify the electronic structure, optical properties, and electrical properties of ZnO NRs (Sugihartono *et al.* 2019). One of the promising dopant elements for functional electronic devices is 3d-transition metal ions (Ti^{2+}, V^{2+}, Cr^{2+}, Mn^{2+}, Fe^{2+}, Co^{2+}, Ni^{2+}, and Cu^{2+}) (Movlarooy *et al.* 2017, Febrianti *et al.* 2017). By introducing the 3d-transition metal ions into the cation sites of the semiconductor crystal lattice, the properties of ferromagnetic and semiconductor will simultaneously present. The semiconducting alloy is called a diluted magnetic semiconductor (DMS) which has potential in spintronic applications (Sugihartono *et al.* 2019). Furthermore, the purpose of DMS is to observe the ferromagnetic behavior at room temperature. On the other hand, some researchers have the intention to increase the photocatalyst activity of ZnO by modifying the electronic structure and the bandgap by incorporating the TM ions into the ZnO structure (Roza *et al.* 2020, Lu *et al.* 2011, Dorneanu *et al.* 2018). The presence of TM ions induces the decreasing of band gap energy and the spin polarization in the structure of ZnO (Ghajari *et al.* 2013). Moreover, among the TM ions, Co^{2+} has high solubility, an ionic radius (0.058 nm) similar to Zn (0.060 nm), and produces a significant redshift, hence tuning of the Fermi level of ZnO (Lu *et al.* 2011, Xiu *et al.* 2006). Others reported that by incorporating Co dopant, the diameter and crystallite size increased, whereas the bandgap decreased (Roza *et al.* 2020). By substitution of Co^{2+} ions into the Zn^{2+} ions, the bandgap energy decreased. It would form the ionization state below the conduction band which allows the transition of the O 2p-orbital to either Co 3d-orbital or Zn 3d-orbital (Xu *et al.* 2010, Chen *et al.* 2021). The presence of Co dopant in the ZnO site is also believed can be used to slow the charge carrier recombination (Demircan *et al.* 2022). Meanwhile, by Co incorporation into the ZnO site, it would improve transparency (Vempati *et al.* 2012). Furthermore, the bandgap of ZnO increases by increasing Co dopants i.e., 3.30eV for non-doped to 3.50eV for Co-doped (Vempati *et*

cobalt (II) acetate tetrahydrate
$C_4H_6CoO_4.4H_2O$

zinc nitrate tetrahydrate
$Zn(NO_3)_2 4H_2O$

1 wt. %
3.5 wt. %
5 wt. %

15 mm × 15 mm glass
substrate coated ZnO seed
layer

0.1 M

Growth
solution

Sealed bottle

Stirrer

Magnetic stirrer

0.1 M

Growth
solution
and glass
substrate

hexamethylenetetramine
$C_6H_{12}N_4$

Non-doped/Co-doped
ZnO nanorods

95°C for 2 hours

Seed layer
Glass substrate

Furnace

Fig. 1 Schematic of synthesis ZnO nanorods by simple low temperature CBD

al. 2012). An increasing bandgap predicts due to the Burstein-Moss effect when Co as a dopant is present (Vempati *et al.* 2012).

In this work, we have synthesized non-doped and Co-doped ZnO NRs using two-step processes, i.e., ultrasonic spray pyrolysis 1.7 MHz (USP) and the simple low-temperature hydrothermal. The USP for deposited ZnO seed layer and the CBD for the growth process of ZnO NRs. Further, we have studied the effect of Co doping on the structural properties of ZnO NRs and observe their absorbance and photoluminescence (PL) properties. Hence, the results have the advantages control the Co as dopants concentration on the structure of ZnO NRs and their optical properties.

2. Experimental details

2.1 Seed layer deposition

We prepared 15 mm×15 mm glass substrate and cleaned it sequentially by putting it into a glass of solvents (acetone, isopropanol, and de-ionized (DI) water). Then, the cleaning process of the glass substrate using each solvent was performed using an ultrasonic bath for 15 minutes. Then, to dry the glass we used the nitrogen blower. For the precursor, we used an analytical grade of zinc acetate dihydrate ($C_4H_6O_4Zn•2H_2O$). To prepare the precursor solution, 0.02 mol of zinc acetate
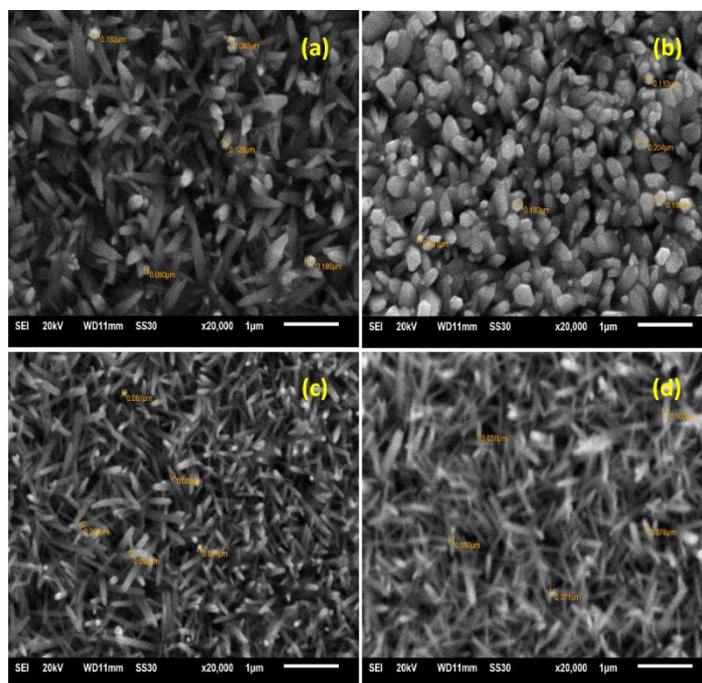
Fig. 2 SEM images of the ZnO NRs (a) Non-doped, (b) Co 1 wt.%, (c) Co 3.5 wt.%, (d) Co 5 wt.%

dihydrate was dissolved in 100 ml of de-ionized (DI) water. The glass substrate was then heated at 450°C. An aerosol of the precursor solution was sprayed and injected on top of indium tin oxide (ITO) glass substrate by the commercial ultrasonic nebulizer (1.7 MHz) for 10 min. Then, we obtain the ZnO thin film as a seed layer.

2.2 Synthesis of ZnO nanorods

Non-doped and Co-doped ZnO NRs were grown on the glass substrate containing the ZnO seed layer using the simple low-temperature chemical bath deposition (CBD) method. Growth solutions were prepared by dissolving zinc nitrate tetrahydrate ($Zn(NO_3)_2 4H_2O$, 99.99%, melting 45°C, Merck) and hexamethylenetetramine ($C_6H_{12}N_4$, 99.99%, melting point 280°C, Merck) in de-ionized (DI) water with the equimolar concentration of 0.1 M by stirring for 30 minutes at room temperature. Then, Cobalt (II) acetate tetrahydrate ($C_4H_6CoO_4.4H_2O$, 98.0-102.0%, melting point 140°C, Merck) was added into the growth solutions as a dopant source with four different weight ratios (0, 1 wt.%, 3.5 wt.%, and 5 wt.%). Next, the solutions were stirred for 60 minutes without any heating until the transparent solution was obtained. The ZnO seed-coated glass substrate was immersed in the growth solution. Furthermore, the growth process of ZnO NRs was performed by heating the sealed bottles at 95°C in the furnace for 2 hours.

2.3 Characterization

To observe the morphology of the non-doped and Co-doped ZnO NRs at room temperature, we performed the scanning electron microscope (SEM) JEOL JSM-6510 at room temperature. The

Table 1 The Atomic percentage of non-doped and Co-doped ZnO NRs

Sample	Atomic percentage of elements (%)		
	Zn	O	Co
Non-doped	57.38	47.62	-
Co 1 wt.%	59.83	40.10	0.08
Co 3.5 wt.%	59.22	40.75	0.02
Co 5 wt.%	53.60	46.29	0.11

structural properties of non-doped and Co-doped ZnO NRs have been characterized by X-ray diffraction (XRD) measurement with CuKα radiation (PAN-analytical). Then, we estimated the structural parameters of the samples such as diffraction angle, lattice parameter, full width at half maximum (FWHM), crystallite size, and microstrain. The optical absorbance of non-doped and Co-doped ZnO NRs was measured using a spectrophotometer UV-Vis MAYA software Spectra-Suite. To estimate the optical band gap energy of non-doped and Co-doped ZnO NRs, we determine it by Tauc plot from the optical absorption edge. Last step, we performed a femtosecond laser (at the excitation wavelength of 325 nm) to study the photoluminescence properties of non-doped and Co-doped ZnO NRs.

3. Results and discussions

3.1 The morphological properties and elemental composition

Figs. 2 (a)-(d) shows scanning electron microscopy (SEM) images of non-doped and Co-doped ZnO NRs with different Co concentrations. As seen from the figure, the morphology of ZnO NRs shows the diameter of Co 1 wt.% has larger than non-doped, Co 3.5 wt.%, and 5 wt.%.

We observed the average diameter of non-doped, Co 1 wt.%, Co 3.5 wt.%, and Co 5 wt.% doped ZnO NRs are 133 nm, 153.4 nm, 73.2 nm, and 75.4 nm, respectively. Furthermore, by energy dispersive x-ray (EDX) spectroscopy, the atomic percentage (at.%) can be analyzed. The atomic percentage of Co 1 wt.%, 3.5 wt.%, and 5 wt.% are 0.08 at.%, 0.02 at.%, and 0.11 at.%, respectively (Table 1).

According to the EDX spectroscopy measurement (Table 1), in a further discussion, we will consider the atomic percentage of Co-doped ZnO NRs. We observed the shape and size of ZnO NRs affected by the dopant concentration of Co. Moreover, the shape and size are more homogeneous when the Co concentration is 0.11at.%. Meanwhile, the Co 0.08 at.% doped ZnO NRs have larger dimensions with an average diameter of 153.4 nm.

3.2 The structural properties of non-doped and Co-doped ZnO NRs

Fig. 3 shows the XRD patterns of non-doped and Co-doped ZnO NRs with different atomic percentages of Co (0.08 at.%, 0.02 at.%, and 0.11 at.%). We observed eight planes (100), (002), (101), (102), (110), (103), (112), and (201) correspond to the angular position (2θ) at 31.663°, 34.412°, 36.181°, 47.441°, 56.478°, 62.766°, 67.850°, and 69.055°, respectively. There are no diffraction peaks from other phases such as CoO, CoO_2, and Co_3O_4 (Vempati *et al.* 2012). We believed it's due to the similarity of the ionic radius (Sugihartono *et al.* 2019), i.e., the ionic radii
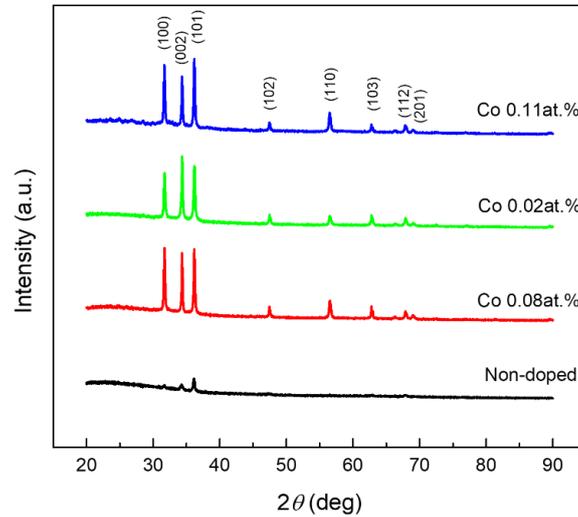
Fig. 3 XRD patterns of non-doped and Co-doped ZnO NRs with different atomic percentages of Co (0.08 at.%, 0.02 at.%, and 0.11 at.%)
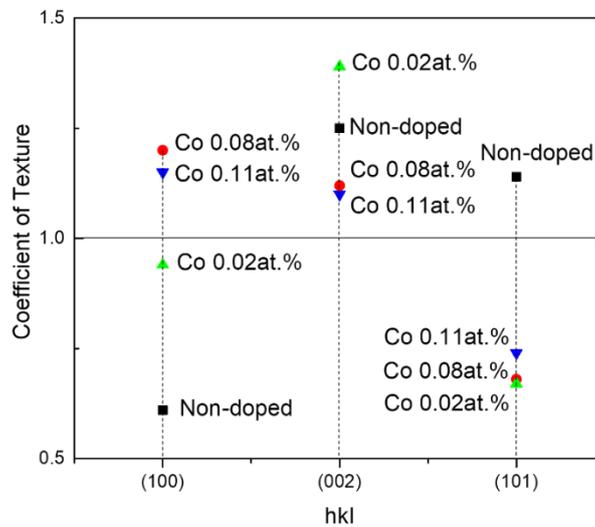
Fig. 4 Coefficient of texture of the non-doped and Co 0.08 at.%, Co 0.02 at.%, and Co 0.11 at.% doped ZnO NRs

of Co and Zn are 0.058 nm and 0.06 nm, respectively (Godavarti *et al.* 2019). Meanwhile, according to International Centre for Diffraction Data (ICDD) number #00-036-1451, the non-doped and Co-doped ZnO NRs possess polycrystalline hexagonal wurtzite structure with the space group P6$_3$mc. Moreover, the preferred orientation of the XRD pattern can be determined by calculating a coefficient of texture (T_{hkl}) (Mohar *et al.* 2020).

$$T_{hkl} = \frac{I(hkl)/I_0(hkl)}{1/n \sum[I(hkl)/I_0(hkl)]} \tag{1}$$

Table 2 The structural parameters of the non-doped and Co 0.08 at.%, Co 0.02 at.%, and Co 0.11 at.% doped ZnO NRs

Sample	2θ	$a=b$ (Å)	c (Å)	d_{hkl} (Å)	FWHM	Crystallite size (nm)	Micro-strain (%)	Volume (Å)
Non-doped	34.354	3.253	5.214	2.615	0.261	35.342	0.590	47.705
Co 0.08 at.%	34.422	3.249	5.206	2.609	0.185	53.849	0.242	47.607
Co 0.02 at.%	34.431	3.249	5.206	2.609	0.191	41.128	0.317	47.592
Co 0.11 at.%	34.425	3.252	5.208	2.609	0.155	58.193	0.224	47.699

As well known, $I(hkl)$ is a measured relative intensity of the reflection from the (hkl) plane; $I_o(hkl)$ is the intensity of the standard reference sample, and n is the total number of reflection peaks of the sample. The T_{hkl} value of non-doped and Co-doped ZnO NRs can be seen in Fig. 4. The T_{hkl} value for the (100) plane was improved by Co incorporation. Meanwhile, the (002) plane has an average value higher than (100) and (101) planes. Hence, we confirmed all the samples have preferred orientation in the (002) plane.

The T_{hkl} values in the (002) plane of non-doped, Co 0.08 at.%, Co 0.02 at.%, and Co 0.11 at.% doped ZnO NRs are 1.25, 1.12, 1.39, and 1.10. These results indicate the preferred orientation of ZnO NRs in the (002) plane can be achieved by a Co-doped of 0.02 at.%. Furthermore, the calculated values of the XRD pattern of non-doped and Co-doped ZnO NRs in the (002) crystal plane, is shown in Table 2.

In the (002) plane the diffraction peak (2θ) shifted slightly to a higher angle by Co incorporation. Furthermore, as compared to non-doped ZnO NRs, the lattice parameters, d_{hkl}, and volume in the (002) plane decreased by the incorporation of Co in the Zn sites. Others reported the lattice parameter of ZnO will decrease when the ionic radius of the dopant is smaller compared to Zn, (Sunwanboon *et al.* 2011). Interestingly, the volume of the unit cell decreases and linearly increases by increasing the atomic percentage of Co. As shown in Table 2, the volume of the unit cell of non-doped, Co 0.08 at.%, Co 0.02 at.%, and Co 0.11 at.% doped ZnO NRs are 47.705 Å, 47.607 Å, 47.592 Å, and 47.699 Å, respectively. It is seen that with a higher atomic percentage of Co (0.11 at.%), the volume of unit cell closed to non-doped ZnO NRs. It's in accordance with Vegard's law that mentioned a higher doping level could increase the volume of the unit cell (Pushpa *et al.* 2017). Further investigation, the non-doped, Co 0.08 at.%, Co 0.02 at.%, and Co 0.11 at.% doped ZnO NRs have the ratio of the unit cell axis length (c/a) are 1.603, 1.602, 1.602, and 1.601, respectively. It is indicating the wurtzite structure of ZnO (Vempati *et al.* 2012). The addition of Co into ZnO causes the value of the full width at half maximum (FWHM) of Co-doped ZnO NRs in the (002) plane to have a narrower peak than non-doped ZnO NRs. The decrease in the FWHM value indicates the crystal quality of ZnO NRs has improved. According to Debye-Scherer's equation, the FWHM can be used to calculate the crystallite size of ZnO NRs (Putri *et al.* 2018). Moreover, the micro-strain of ZnO NRs calculated by using the Stokes-Wilson equation (Mohar *et al.* 2020). The crystallite size and the micro-strain of non-doped, Co 0.08 at.%, Co 0.02 at.%, and Co 0.11 at.% doped ZnO NRs are 35.342 nm, 53.849 nm, 41.128 nm, and 58.193 nm, respectively. On the other hand, the micro-strain of non-doped, Co 0.08 at.%, Co 0.02 at.%, and Co 0.11 at.% doped ZnO NRs are 0.590%, 0.242%, 0.317%, and 0.224%, respectively. It is confirmed that the crystallite size and micro-strain changed Co incorporation in the ZnO NRs structure.
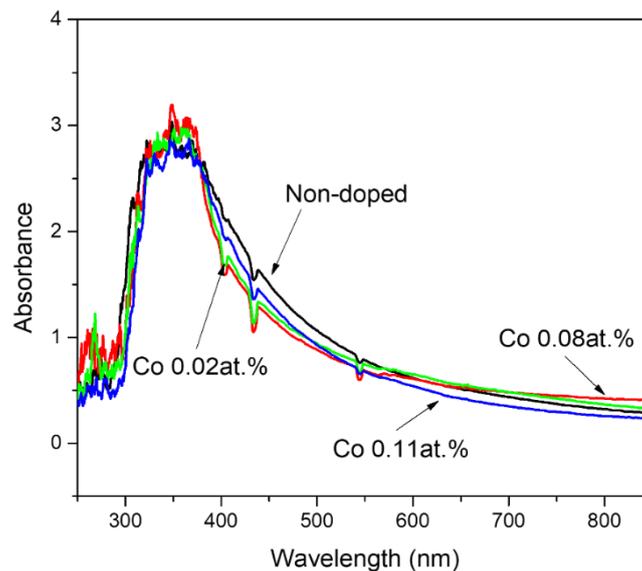
Fig. 5 UV-Vis absorbance spectra of the non-doped and Co 0.08 at.%, Co 0.02at.%, and Co 0.11 at.% doped ZnO NRs

3.3 The optical properties of non-doped and Co-doped ZnO NRs

Fig. 5 shows ultraviolet-visible (UV-Vis) absorbance spectra of non-doped and Co-doped ZnO NRs with different Co concentrations.

The optical absorption spectra of the ZnO NRs recorded in the range of 250-850 nm. The absorption spectra of non-doped and Co 0.08 at.%, Co 0.02 at.%, and Co 0.11 at.% doped ZnO NRs have a broad peak in the range of 300-550 nm with strong absorption in the range of UV wavelength and weak absorption in the range of visible. There is an increase in intensity in the range of UV wavelength with the most intense peak for Co 0.08 at.% doped ZnO NRs at ~350 nm. It indicates the characteristic of a wide bandgap ZnO (Sugihartono, *et al.* 2015). Moreover, as seen in Fig. 5, the optical absorption of the Co 0.08 at.% doped ZnO NRs has stronger intensity may be due to it has larger dimension as confirmed by the scanning electron microscopy (SEM) images (Fig. 2). Furthermore, the broad absorbance and the intensity smoothly decrease up to near-infrared wavelength. In contrast, most of the absorbance spectra of ZnO NRs have a sharp absorption edge (Roza *et al.* 2020, Febrianti, *et al.* 2017, Šutka *et al.* 2016). Hence, our results indicate the native defects of ZnO NRs spread simultaneously. Meanwhile, the presence of the Co dopant in the ZnO NRs structure suppresses the native defects in the forbidden bandgap.

The bandgap of non-doped and Co-doped ZnO NRs can be estimated using the Tauc plot from the optical absorption edge. Fig. 6 shows the Tauc plot for the non-doped and Co 0.08 at.%, Co 0.02 at.%, and Co 0.11 at.% doped ZnO NRs where the absorption coefficient times the photon energy to the second power plotted versus the incident photon energy (Wang *et al.* 2008, Viezbicke *et al.* 2015).

The bandgap energy (E_g) non-doped and Co-doped ZnO NRs estimated by drawing the intersection of the tangent from the curves. It is seen that the incorporation of Co into ZnO NRs induces the change of bandgap energy. We observed the *Eg* of non-doped was found to be 3.066
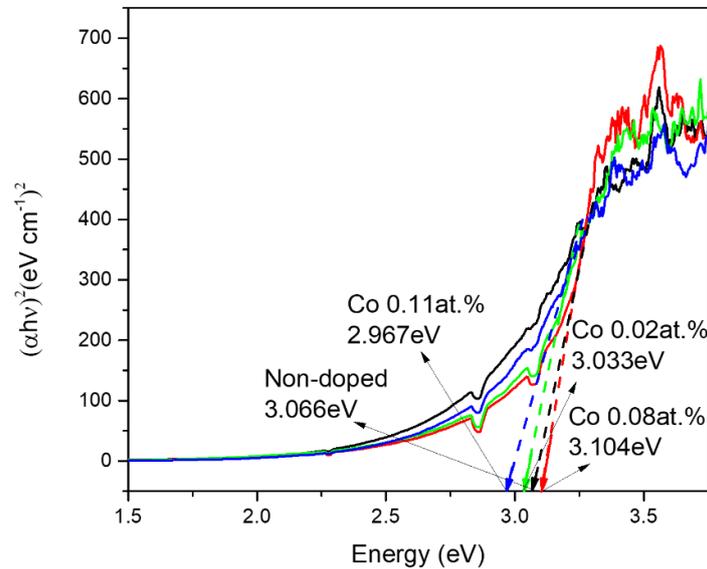
Fig. 6 Optical Bandgap energy of the non-doped and Co 0.08 at.%, Co 0.02 at.%, and Co 0.11 at.% doped ZnO NRs

eV. Meanwhile, for the Co 0.02 at.% and Co 0.11 at.% doped ZnO NRs, the E_g decreased to 3.033 eV and 2.967 eV, respectively. It is relevant to the other report, the E_g of ZnO decreases by Co doping concentrations (Majeed-Khan *et al.* 2010). The redshift of the E_g for Co 0.02 at.%, and Co 0.11 at.% doped ZnO NRs may occur due to modification on the lattice dimensions (Qiu *et al.* 2006). Meanwhile, others reported that the bandgap energy reduction is due to the introduction of new unoccupied states by Co 3d electrons which cause the exchange interactions between the Co electrons in the d orbitals and the electrons in the s orbitals of O_2 and the *p* orbitals of Zn (Roza *et al.* 2020). It is relevant to the theoretical result that the introducing TM ions in the ZnO site, the d band will have high localization compared to the *s* and *p* bands (Ghajari *et al.* 2013). By the presence of Co as a ferromagnetic dopant in the ZnO structure, the *sp-d* exchange interaction expecting occurs between the band electrons and the localized d electrons of Co^{2+} (Shindu *et al.* 2019). The *sp-d* hybridization is located lowers the bottom of the conduction band. Meanwhile, there is a blueshift of E_g (3.104 eV) by Co 0.08 at.% doped ZnO NRs. This blueshift energy by Co incorporation in ZnO structure can be described in terms of the Burstein-Moss effect (Vempati *et al.* 2012). As reported, the increasing value of Eg of ZnO NRs depends on several factors such as grain size, carrier concentration, and lattice strain (Pushpa *et al.* 2017). However, we predict the Co-doped NRs with the Co atomic percentage of 0.08 % may occur the increasing carrier concentration in the bottom of the conduction band. Hence, it causes the Fermi level to shift. Hence, the Burstein-Moss effect compensates the exchange interaction *sp-d* transition state.

The photoluminescence (PL) spectra of the non-doped and Co-doped ZnO NRs (Co 0.08 at.%, Co 0.02 at.%, and Co 0.11 at.%) at room temperature are presented in Fig. 7.

As can be seen in the figure, the PL spectra of ZnO NRs exhibited two typical emissions, i.e., excitonic-relates ultraviolet (UV) and defect-related green band (GB) emissions which correspond to near band-edge emission (NBE) and deep-level emission (DLE), respectively. To evaluate the structural defects of ZnO, we have calculated the ratio of UV and GB (UV/GB) (Sugihartono, *et*
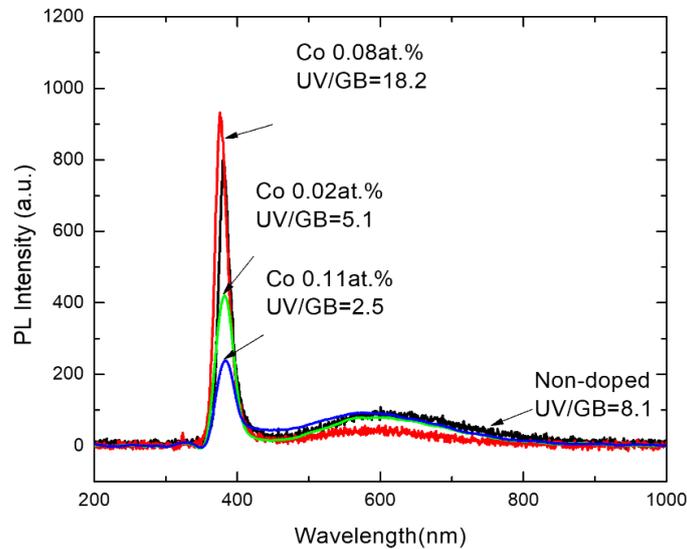
Fig. 7 The PL spectra of the non-doped and Co 0.08 at.%, Co 0.02 at.%, and Co 0.11 at.% doped ZnO NRs at room temperature
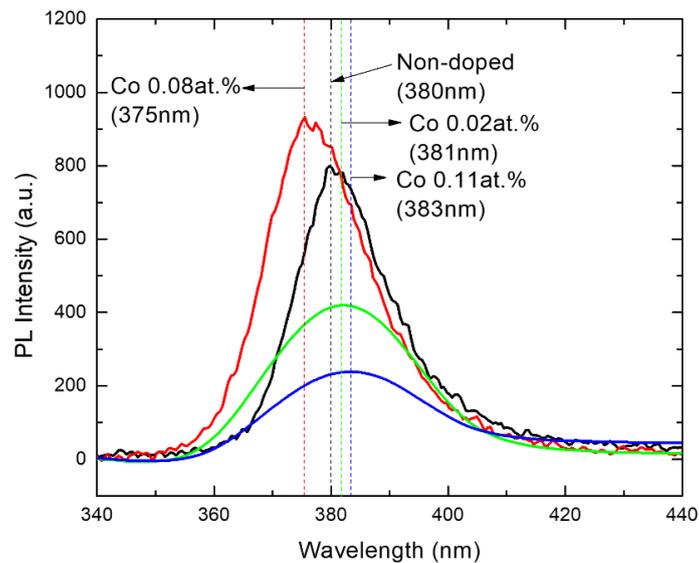
Fig. 8 The shift of NBE emission in the Co-doped ZnO NRs with different atomic composition

al. 2015, Tan *et al.* 2006). The UV/GB value for Co 0.08 at.% doped ZnO NRs is 18.2. This value is higher than the non-doped ZnO NRs, Co 0.02 at.%, and Co 0.11 at.% doped ZnO NRs. To the best of our knowledge, the GB emission is mostly due to radiative recombination of photogenerated holes with electrons in a singly oxygen vacancy (Sugihartono *et al.* 2016, Tan *et al.* 2006). However, others reported that by Co incorporation into the ZnO structure, there is the d-d transition of Co^{2+} ions which contributes to GB emission (Shindu *et al.* 2019). A further

observation from the PL spectra shows the blueshift of the NBE emission for the Co 0.11 at.% doped ZnO NRs (Fig. 8). As well known, the Co incorporation affects the distribution of the internal defects in the ZnO NRs. Furthermore, by Co incorporating, there is substitution Zn by Co ions which cause the increasing electron carrier concentration (Demircan *et al.* 2023).

This phenomenon is called Burstein-Moss effect. The blueshift of NBE emission may be attributed to the Burstein-Moss effect (Mohar *et al.* 2020, Toufiq *et al.* 2006). On the other hand, for Co 0.02 at.%, and Co 0.08 at.% doped ZnO NRs indicate a redshift of the NBE emission. The redshift may correlate with the bandgap shifting as a function of lattice volume and contribution to the exchange energy due to Co incorporation (Qiu *et al.* 2006).

4. Conclusions

In summary, we have studied the structural and optical properties of the non-doped and Co 0.08 at.%, Co 0.02 at.%, and Co 0.11 at.% doped ZnO NRs synthesized using the simple low-temperature CBD method at 95°C for 2 hours.
• The morphology of ZnO NRs influenced by Co incorporation.
• The XRD pattern of non-doped and Co-doped ZnO NRs have the preferred orientation in the (002) plane and possess polycrystalline hexagonal wurtzite structure with the space group P63mc.
• The proper Co concentration in the ZnO structure provides a larger NRs dimension and the Co 0.08 at.% doped ZnO NRs has stronger absorption and blueshift bandgap energy (3.104 ev).
• The room temperature PL spectra of ZnO NRs exhibited two typical emissions, i.e., excitonic-relates ultraviolet (UV) and defect-related green band (GB) emissions.
• The Co-doped ZnO NRs induce a blueshift of NBE emission due to the Burstein-Moss effect. Meanwhile, the redshift of NBE emission is attributed to the modification of the lattice dimensions and exchange energy.

Acknowledgments

References

Allahverdinejad Sarab, V. and Movlarooy, T. (2022), "Structural and electronic properties of double-walled zigzag and armchair Zinc oxide nanotubes", *Chin. J. Phys.*, **83**, 571-578. https://doi.org/10.1016/j.cjph.2022.08.004.

Chen, Z., Fang, Y., Wang, L., Chen, X., Lin, W. and Wang, X. (2021), "Remarkable oxygen evolution by Co-doped ZnO nanorods and visible light", *Appl. Catal. B: Environ.*, **296**, 120369. https://doi.org/10.1016/j.apcatb.2021.120369.

Demircan, G., Acikgoz, A., Yalcin, S., Aytar, E., Balak, M.V. and Aktas, B. (2023), "the influence of doping perimidine ruthenium complexes on structural, optic, and residual stress properties of ZnO thin films",

Brazil. J. Phys., **53**, 1-11. https://doi.org/10.1007/s13538-022-01245-x.

Demircan, G., Gurses, E.F., Aktas, B., Yalcin, S., Acikgoz, A., Aytar, E., Ceyhan, G. and Aktas, B. (2023), "Sol-gel synthesis of Si-ZnO, Ti-ZnO and Si-Ti-ZnO thin films: Impact of Si and Ti content on structural and optical properties", *Mater. Today Commun.*, **34**, 105234. https://doi.org/10.1016/j.mtcomm.2022.105234.

Demircan, G., Yalcin, S., Alivi, K., Ceyhan, G., Acikgoz, A., Balak, M.V., Aktas, B. and Das, R. (2022), "The effect of Co and Mn Co-Doping on structural and optical properties of ZnO thin films", *Opt. Mater.*, **126**, 112163. https://doi.org/10.1016/j.optmat.2022.112163.

Dorneanu, P.P., Tudose, I.V., Suchea, M., Koudoumas, E., Fifere, N. and Airinei, A. (2018), "Preparation and characterization of Ni, Co doped ZnO nanoparticles for photocatalytic applications", *Appl. Surf. Sci.*, **448**, 481-488. https://doi.org/10.1016/j.apsusc.2018.04.124.

Febrianti, Y., Putri, N.A., Sugihartono, I., Fauzia, V. and Handoko, D. (2017), "Synthesis and characterization of Co-doped zinc oxide nanorods prepared by ultrasonic spray pyrolysis and hydrothermal methods", *AIP Conf. Proc.*, **1862**(1), 030056. https://doi.org/10.1063/1.4991160.

Ghazari, N., Kompany, A., Movlarooy, T., Roozban, F. and Majidiyan, M. (2013), "Synthesis, experimental and theoretical investigations of Zn 1-xCu xO nanopowders", *J. Magnet. Magnetic Mater.*, **325**, 42-46. http://doi.org/10.1016/j.jmmm.2012.08.008.

Godavarti, U., Mote, V.D., Reddy, M.R., Nagaraju, P., Kumar, Y.V., Dasari, K.T. and Dasari, M.P. (2019), "Precipitated cobalt doped ZnO nanoparticles with enhanced low temperature xylene sensing properties", *Physica B: Condens. Matt.*, **553**, 151-160. https://doi.org/10.1016/j.physb.2018.10.034.

Iwan, S., Dianisya, D., Fahdiran, R., Budi, E., Susila, A.B. and Handoko, E. (2019), "Morphological, structural, and optical properties of Co-doped ZnO NPs prepared by precipitation method", *J. Ceram. Proc. Res.*, **20**(5), 518-521. https://doi.org/10.36410/jcpr.2019.20.5.518.

Iwan, S., Zhao, J.L., Tan, S.T., Bambang, S., Hikam, M., Fan, H.M. and Sun, X.W. (2015), "Ion-dependent electroluminescence from trivalent rare-earth doped n-ZnO/p-Si heterostructured light-emitting diodes", *Mater. Sci. Semicond. Proc.*, **30**, 263-266. https://doi.org/10.1016/j.mssp.2014.09.048.

Jin, C., Yuan, X., Ge, W., Hong, J. and Xin, X. (2003), "Synthesis of ZnO nanorods by solid state reaction at room temperature", *Nanotechnol.*, **14**(6), 667-669. https://doi.org/10.1088/0957-4484/14/6/319.

Lehru, R., Radhanpura, J., Kumar, R., Zala, D., Vadgama, V.S., Dadhich, H., ... & Solanki, P.S. (2021), "Studies on electrical properties of Fe doped ZnO nanostructured oxides synthesized by sol-gel method", *Solid State Commun.*, **336**, 114415. https://doi.org/10.1016/j.ssc.2021.114415.

Lima, S.A.M., Sigoli, F.A., Miguel, J. and Davolos, M. (2001), "Luminescent properties and lattice defects correlation on zinc oxide", *Int. J. Inorgan. Mater.*, **3**(7), 749-754. https://doi.org/10.1016/S1466-6049(01)00055-1.

Lu, Y., Yanhong, L., Wang, D., Wang, L., Xie, T. and Jiang, T. (2011), "A high performance cobalt-doped ZnO visible light photocatalyst and its photogenerated charge transfer properties", *Nano Res.*, **4**(11), 1144-1152. https://doi.org/10.1007/s12274-011-0163-4.

Majeed-Khan, M., Wasi-Khan, M., Alhoshan, M., AlSalhi, M. and Aldwayyan A. (2010), "Influences of Co doping on the structural and optical properties of ZnO nanostructured", *Appl. Phys. A*, **100**(1), 45-51. https://doi.org/10.1007/s00339-010-5840-8.

Ming-Dong, W., Dao-Yun, Z., Yi, L., Lin, Z., Chang-Xi, Z., Zhen-Hui, H., ... & Li-Shi, W. (2008), "Determination of thickness and optical constants of ZnO thin films prepared by filtered cathode vacuum arc deposition", *Chin. Phys. Lett.*, **25**(2), 743-746. https://doi.org/10.1088/0256-307X/25/2/106.

Mohar, R.S., Sugihartono, I., Fauzia, V. and Umar, A. (2020), "Dependence of optical properties of Mg-doped ZnO nanorods on Al dopant", *Surf. Interf.*, **19**, 100518. https://doi.org/10.1016/j.surfin.2020.100518.

Movlarooy, T. (2017), "Transition metals doped and encapsulated ZnO nanotubes: Good materials for the spintronic applications", *J. Magnet. Magnetic Mater.*, **441**, 139-148. https://doi.org/10.1016/j.jmmm.2017.05.055.

Movlarooy, T. (2018), "Study of quantum confinement effects in ZnO nanostructures", *Mater. Res. Expr.*, **5**, 035032. https://doi.org/10.1088/2053-1591/aab389

Pushpa, N. and Kokila, M. (2017), "Effect of cobalt doping on structural, thermo and photoluminescent properties of ZnO nanopowders", *J. Lumines.*, **190**, 100-107. https://doi.org/10.1016/j.jlumin.2017.05.032.

Putri, N.A., Fauzia, V., Sugihartono, I., Roza, L., Umar, A. and Budi, S. (2018), "Mn-doping-induced photocatalytic activity enhancement of ZnO nanorods prepared on glass substrates", *Appl. Surf. Sci.*, **439**, 285-297. https://doi.org/10.1016/j.apsusc.2017.12.246.

Qiu, X., Li, L. and Li, G. (2006), "Nature of the abnormal band gap narrowing in highly crystalline Zn1−xCoxO nanorods", *Appl. Phys. Lett.*, **88**(11), 114103. https://doi.org/10.1063/1.2185617.

Roza, L., Febrianti, Y., Sugihartono, I. and Fauzia, V. (2020), "The role of cobalt doping on the photocatalytic activity enhancement of ZnO nanorods under UV light irradiation", *Surf. Interf.*, **18**, 100435. https://doi.org/10.1016/j.surfin.2020.100435.

Shindu, H.S., Kulkarni, S.D., Choudhary, R.J., Babu, P.D. and Rajendra, B.V. (2019), "Influence of cobalt doping on structure, optical and magnetic properties of spray pyrolysed nano structured ZnO films", *Physica B: Condens. Matter.*, **572**, 18-26. https://doi.org/10.1016/j.physb.2019.07.034.

Song, J. and Lim, S. (2006), "Effect of seed layer on the growth of ZnO nanorods", *J. Phys. Chem. C*, **111**(2), 596-600. https://doi.org/10.1021/jp0655017.

Sugihartono, I., Fauzia, V., Azeti, R.A., Maharani, M., Fahdiran, R. and Budi, E. (2019), "Morphology and optical properties of Cu-Al co-doped ZnO nanostructures", *Surf. Interf.*, **16**, 147-151. https://doi.org/10.1016/j.surfin.2019.05.009.

Sugihartono, I., Fauzia, V., Umar, A. and Sun, X. (2016), "Room temperature photoluminescence properties of ZnO nanorods grown by hydrothermal reaction", *AIP Conf. Proc.*, **1729**, 020031. https://doi.org/10.1063/1.4946934.

Sugihartono, I., Soegijono, B., Zhao, J.L., Tan, S.T., Fan, H.M., Sun, L., et al. (2012), "Green electroluminescence from an n-ZnO: Er/p-Si heterostructured light-emitting diode", *Physica B: Condens. Matt.*, **407**(14), 2721-2724. https://doi.org/10.1016/j.physb.2012.03.072.

Sugihartono, I., Zhao, J.L., Tan, S.T. and Sun, X. (2018), "Enhancement of UV photoluminescence in ZnO tubes grown by metal organic chemical vapour deposition (MOCVD)", *Vacuum*, **155**, 408-411. https://doi.org/10.1016/j.vacuum.2018.06.035.

Šutka, A., Käämbre, T., Pärna, R., Juhnevica, I., Maiorov, M., Joost, U. and Kisand, V. (2016), "Co doped ZnO nanowires as visible light photocatalysts", *Solid State Sci.*, **56**, 54-62. https://doi.org/10.1016/j.solidstatesciences.2016.04.008.

Suwanboon, S., Amornpitoksuk, P. and Sukolrat, A. (2011), "Dependence of optical properties on doping metal, crystallite size and defect concentration of M-doped ZnO nanopowders (M=Al, Mg, Ti)", *Ceram. Int.*, **37**(4), 1359-1365. https://doi.org/10.1016/j.ceramint.2010.12.010.

Ta, Q.T.H., Namgung, G. and Noh, J.S. (2018), "Morphological evolution of solution-grown cobalt-doped ZnO nanostructures and their properties", *Chem. Phys. Lett.*, **700**, 1-6. https://doi.org/10.1016/j.cplett.2018.04.002.

Tan, S.T., Chen, B.J., Sun, X., Hu, X., Zhang, X. and Chua, S. (2005), "Properties of polycrystalline ZnO thin films by metal organic chemical vapor deposition", *J. Crystal Growth.*, **281**(2-4), 571-576. https://doi.org/10.1016/j.jcrysgro.2005.04.093.

Tan, S.T., Chen, B.J., Sun, X.W., Fan, W.J., Kwok, H.S., Zhang, X.H. and Chua, S.J. (2005), "Blueshift of optical band gap in ZnO thin films grown by metal-organic chemical-vapor deposition", *J. Appl. Phys.*, **98**(1), 013505. https://doi.org/10.1063/1.1940137.

Tan, S.T., Sun, X.W., Zhang, X.H., Chua, S.J., Chen, B.J. and Teo, C.C. (2006), "Cluster coarsening in zinc oxide thin films by postgrowth annealing", *J. Appl. Phys.*, **100**(3), 033502. https://doi.org/10.1063/1.2218468.

Toufiq, A.M., Hussain, R., Shah, A., Mahmood, A., Rehman, A., Khan, A. and ur Rahman, S. (2021), "The influence of Mn doping on the structural and optical properties of ZnO nanostructures", *Physica B: Condens. Matt.*, **604**, 412731. https://doi.org/10.1016/j.physb.2020.412731.

Vempati, S., Shetty, A., Dawson, P., Nanda, K. and Krupanidhi, S. (2012), "Solution-based synthesis of cobalt-doped ZnO thin films", *Thin Solid Film.*, **524**, 137-143. https://doi.org/10.1016/j.tsf.2012.10.008.

Viezbicke, B., Patel, S., Davis, B. and Birnie, D. (2015), "Evaluation of the Tauc method for optical absorption edge determination: ZnO thin films as a model system", *Physica Status Solidi (b)*, **252**(8), 1700-1710. https://doi.org/10.1002/pssb.201552007.

Xu, C., Cao, L., Su, G., Liu, W., Qu, X. and Yu, Y. (2010), "Preparation, characterization and photocatalytic activity of Co-doped ZnO powders", *J. Alloy. Compound.*, **497**(1-2), 373-376. https://doi.org/10.1016/j.jallcom.2010.03.076.

Yang, Y.H., Chen, X.Y., Feng, Y. and Yang, G. (2007), "Physical mechanism of blue-shift of UV luminescence of a single pencil-like ZnO nanowire", *Nano Lett.*, **7**(12), 3879-3883. https://doi.org/10.1021/nl071849h.

Yu, H., Li, J., Loomis, R.A., Gibbons, P., Wang-wang, L. and Buhro, W. (2003), "Cadmium selenide quantum wires and the transition from 3d to 2d Confinement", *J. Am. Chem. Soc.*, **125**(52), 16168-16169. https://doi.org/10.1021/ja037971.

CC